Transport in Porous Media **40:** 201–218, 2000.

The Motion of Long Bubbles in a Network of Tubes

JAN STARK[1] and MICHAEL MANGA[2,⋆]
[1]*Département des Sciences de la Matière, Ecole Normale Supérieure de Lyon, Lyon, France*
[2]*Department of Geological Sciences, University of Oregon, Eugene, OR 97403, U.S.A.*

(Received: 15 January 1999; in final form: 26 October 1999)

Abstract. The motion and interaction of discrete bubbles in porous materials is studied numerically using a network model. The goal is to extend analytical results for the motion of bubbles through a single straight tube to a more 'realistic' geometry for porous materials, modeled here as a planar network of straight tubes of different radii. The problem is characterized by two dimensionless parameters, the capillary number (Ca) and the volume fraction of bubbles (ϕ); results are characterized by determining the effective permeability of the network and the mean residence time of bubbles in the material. The simulations indicate that at low volume fraction most of the bubbles follow a limited number of high-flow pathways through the network. In this case the predictions of our simulations can be approximated by a simple analytical model. Bubbles interact with each other because their presence changes the local resistance to flow in individual tubes. As ϕ increases, interactions between individual bubbles become important resulting in a wider range of residence times in the porous material.

Key words: two-phase flow, bubbles, network simulation, effective permeability.

1. Introduction

Multiphase transport processes in porous materials are encountered in many branches of science and engineering. Under various circumstances one of the phases can exist in the form of dispersed discrete droplets, defining the so-called 'drop-traffic flow' limit (e.g., Avraam and Payatakes, 1995). Here we focus on the specific limit in which the dispersed phase consists of bubbles. Suspensions of air bubbles in water can be used to introduce oxygen into groundwater in order to enhance bioremediation efforts (e.g., Fry *et al.*, 1997), and have also been used to remove volatile organic compounds from contaminated soils (e.g., Gudemann and Hiller, 1988; Böhler *et al.*, 1990). High volume fraction suspensions (foams) have applications to enhanced oil recovery and hazardous waste management (Olbricht, 1996).

The motion of drops and bubbles in straight and constricted tubes is frequently studied as a model for pore-scale processes (e.g., Martinez and Udell, 1990; Olbricht and Kung, 1992; Tsai and Miksis, 1994). While such model geometries are obviously gross over-simplifications of true pore geometries, the effects

⋆ Author for correspondence: tel.: 541-346-5574; fax: 541-346-4692;
e-mail: manga@newberry.uoregon.edu

of bounding walls, viscosity ratio, volume fraction, drop volume, and interfacial tension can all be considered and may thus provide insight into pore-scale hydrodynamics. In the simulations reported here, our goal is to extrapolate analytical results for the motion of bubbles in straight tubes to a geometry more appropriate for porous materials that consists of a network of intersecting tubes. We can thus account for 'a fundamentally important topological characteristic of porous solids, namely, interconnectedness of the pore space' (Celia *et al.*, 1995). The approach we follow here is similar to that used in previous network studies of multiphase flow (e.g., Koplik and Lasseter, 1982; Dias and Payatakes, 1986; Rajaram *et al.*, 1997) though our focus is on the less well-studied limit (e.g., Constantinides and Payatakes, 1996) of steady-state conditions. Here, we consider only the motion of discrete non-wetting bubbles so that we can focus on hydrodynamic processes.

The presence of a bubble in a pore affects the flow in that pore. Thus, as bubbles pass through a porous material the local resistance to flow in each pore changes with time. Bubbles, therefore, can interact with each other by changing the spatial distribution of pressure gradients and flow, and network simulations allow us to determine the importance of nodes in flow pathways. Because of the nonlinear relationship between the pressure drop across a bubble and the speed of the bubble, our problem is nonlinear and computational requirements limit us to considering networks with less than a few hundred tubes. Nevertheless, we are able to simulate large enough networks to determine the effect of model parameters on flow and bubble motion.

2. Model

We begin by reviewing some 'classical' results on the movement of a single bubble and a train of bubbles in single straight tube. We then use these results to construct a theoretical model of bubble-traffic flow. We consider only the motion of discrete bubbles that are separated from pore walls by a thin film of fluid. We can thus focus entirely on hydrodynamic processes and ignore contact line dynamics and other physicochemical processes. The approach is conceptually similar to that in droplet train models (e.g., Foulser *et al.*, 1991; Babchin and Yuan, 1997), however, the bubbles are not required to move at the same speed as the fluid.

2.1. THE MOTION OF LONG BUBBLES IN A TUBE

Consider the forced, steady displacement of a bubble in a tube. The viscosity of the bubble is assumed to be negligible and the Reynolds number of the associated liquid displacement is small. In the limit that the bubble is infinitely long, Bretherton (1961) found that the speed of the bubble u exceeds the average speed of the suspending fluid by an amount uw, with

$$w \simeq 1.29(3\mathrm{Ca})^{2/3} \quad \text{as} \quad \mathrm{Ca} \to 0. \tag{1}$$

Here, Ca denotes the capillary number

$$\mathrm{Ca} = \frac{\mu u}{\sigma}, \tag{2}$$

where μ is the dynamic viscosity of the suspending fluid, and σ is the interfacial tension between the bubble and suspending fluid. The pressure drop ΔP_b across the bubble is given by

$$\Delta P_\mathrm{b} \simeq 3.58 \frac{\sigma}{r} (3\mathrm{Ca})^{2/3} \quad \text{as} \quad \mathrm{Ca} \to 0, \tag{3}$$

where r is the radius of the tube.

Ratulowski and Chang (1989) found the next-order correction to Equation (3):

$$\Delta P_\mathrm{b} \simeq \frac{\sigma}{r} [3.58(3\mathrm{Ca})^{2/3} - 9.07\mathrm{Ca}^{0.95}]. \tag{4}$$

Bretherton's first-order approximation is a useful approximation up to $\mathrm{Ca} \simeq 10^{-2}$, whereas the second-order approximation of Ratulowski and Chang can be useful for Ca up to 10^{-1}. Ratulowski and Chang (1989) also extended Bretherton's analysis to bubbles of finite length and found that the above results for infinite bubbles are adequate approximations for bubbles with volumes V_b larger than V_c:

$$V_\mathrm{b} > V_\mathrm{c} = \tfrac{4}{3}\pi r^3, \tag{5}$$

where r is the radius of the tube. Furthermore, numerical and experimental results show that the speed of infinitely long bubbles is a good approximation for bubbles of finite length if $V_\mathrm{b} > 0.95 V_\mathrm{c}$ (Olbricht, 1996). Finally, Ratulowski and Chang (1989) studied trains of identical bubbles in a tube and concluded that each bubble in such a train behaves as an isolated bubble. The results of Ratulowski and Chang thus justify the use of Bretherton's formulas to construct a model of bubble flow in a network of tubes.

Other related studies have considered the effects of the presence of surfactants (Ratulowski and Chang, 1990; Borhan and Mao, 1992), a finite viscosity of the non-wetting fluid (Teletzke *et al.*, 1988), and the motion of bubbles in noncircular tubes (e.g., Wong *et al.*, 1995a,b). The motion of long gas bubbles is strongly affected by surfactant on the interface (He *et al.*, 1991). Indeed, Marangoni stresses and changes in the boundary conditions on the surface of the bubbles, both due to the presence of surfactant, can account for the difference between theoretical results and experimental measurements (Olbricht, 1996). These results could, in principle, be used in place of those of Bretherton (1961) in our model.

The thickness h_0 of the film between the tube wall and bubble is

$$h_0 = 0.643 r (3\mathrm{Ca})^{2/3}. \tag{6}$$

Nonhydrodynamic forces, such as van der Waals forces, typically become dynamically important for lengthscales less than about 10–100 nm. For a tube with

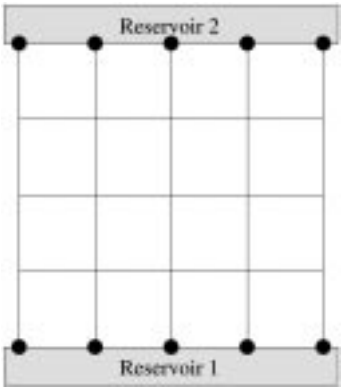

Figure 1. Network of tubes for $d = 4$.

$r = 1$ mm, nonhydrodynamic effects should thus be negligible for Ca $>$ O(10^{-6}). We also assume that the motion of the bubbles makes the film hydrodynamically stable, and suppresses gravitational and capillary instabilities (e.g., Babchin *et al.*, 1983; Frenkel *et al.*, 1987). At Ca greater than some critical value, typically ≈ 1, bubbles can undergo transient deformations and break into smaller bubbles (e.g., Olbricht and Kung, 1992; Borhan and Pallinti, 1999).

2.2. MODEL DESCRIPTION

We represent the porous medium by a network of tubes (see Figure 1) across which an applied pressure difference transports the bubbly liquid from reservoir 1 to reservoir 2. We perform simulations in square networks of different sizes. We define the dimension d of the network as the number of tubes on the sides that are not formed by the reservoirs so that the total number of tubes is $2d^2$. The dimension of the network in Figure 1 is thus four.

Tube radii are chosen by a random number generator according to the distribution shown in Table I; the standard deviation is $1/4$ of the mean value ($\bar{r}$). We let the tube length be a constant equal to 21.8 times the mean tube radius. The distribution of radii and relative tube length are the same as those used in the experimental study of Avraam and Payatakes (1995).

The model is characterized by two physical parameters, the capillary number (Ca), and the volume fraction of bubbles (ϕ). Because u in Equation (2) is not a constant in the network, we define the 'overall capillary number' $\overline{\text{Ca}}$ as the average

Table I. Probability distribution of tube radii ($\bar{r}$ is the mean tube radius)

Radius	$\bar{r}/2$	$3\bar{r}/4$	$\bar{r}$	$5\bar{r}/4$	$3\bar{r}/2$
Frequency of appearance (%)	16	21	26	21	16

of Ca over all tubes that contain bubbles. In our simulations, we assume that all the bubbles have the same volume V_b. For the Bretherton (1961) results to apply for all bubbles, the bubble volume must be smaller than the volume of the thinnest tube and greater than $0.95V_c$ in the widest tube (Olbricht, 1996). We use the value $V_b = 4\pi(1.5\bar{r})^3/3$ for all bubbles in all of our simulations. The time-dependent average time T between two bubbles entering the network at one of the $d+1$ entrance points is determined by ϕ – a fixed parameter for each simulation – and the time-dependent total flux. We use random numbers to generate a distribution of times between two bubbles with all times between $4T/5$ and $6T/5$ being equally probable.

At small Reynolds numbers, the discharge Q of a fluid through a straight circular tube of length l is given by

$$Q = \frac{\pi\rho r^4}{8\mu l}\Delta P, \tag{7}$$

where ΔP is the pressure difference across the tube, and ρ is the fluid density. For a tube containing bubbles, the discharge becomes

$$Q = \frac{\pi\rho r^4}{8\mu l^*}\left[\Delta P - \sum_{\text{bubbles}} \Delta P_b(Q)\right], \tag{8}$$

where l^* is the length of the tube minus the lengths of the bubbles in it, and $\Delta P_b(Q)$ is the pressure drop across one bubble, given by (3). Note that ΔP_b depends on Ca. Ca, in turn, depends on the average speed of the bubble in the tube. The speed of the bubbles u is related by

$$v = (1-w)u \tag{9}$$

to the average speed of the suspending (wetting) fluid v, which is given by

$$v = \frac{Q}{\rho\pi r^2}\,. \tag{10}$$

Thus, ΔP_b depends on Q, and so does w. Substituting (9) and (10) into (1) yields

$$w(1-w)^{2/3} = \tau \tag{11}$$

with

$$\tau = 1.29\left(\frac{3\mu}{\sigma}\frac{1}{\rho\pi r^2}\right)^{2/3} Q^{2/3}. \tag{12}$$

Expansion into a power series gives, to the second order,

$$w = \tfrac{3}{4}\left(1 - \sqrt{1 - \tfrac{8}{3}\tau}\right). \tag{13}$$

Thus, ΔP_b can be obtained using (13), (1) and (3).

We can write Equation (8) in the form

$$Q = \underbrace{\frac{\pi \rho r^4}{8 \mu l^*} \left[1 - \sum_{\text{bubbles}} \frac{\Delta P_{\text{b}}(Q)}{\Delta P} \right]}_{\text{conductivity}} \Delta P. \tag{14}$$

In this form, we can see the analogy between the discharge through a tube and the electric current through a conductor. The conductivity, however, depends on the discharge and the pressure drop. The tube can thus be compared to an electrical conductor whose conductivity depends on the current and the voltage drop. The nonlinearity of (14), a feature not characteristic of some multiphase network models (e.g., Constantinides and Payatakes, 1996; Rajaram *et al.*, 1997), provides some numerical challenges and limits the size of d and the number of tubes. Numerical details are provided in the Appendix.

We monitor the position of each bubble in the network. The equations described previously are used to calculate the flux in all of the tubes for a given configuration of bubbles. We then calculate the time it would take for each of the bubbles to reach the end of a tube, and advance all the bubbles the distance defined by their respective speeds multiplied by the shortest of these times. We thus arrive at a situation where at least one of the bubbles has reached a node in the network. Once again, we use random numbers to determine which new tube the bubble will enter. The probability of going into a given tube is assumed to be proportional to the flux in that tube. The results of experimental and numerical studies on the partitioning of particles and drops at bifurcations indicate that the actual distribution is more complicated and depends on the form of the node and the particle volume fraction (e.g., Ditchfield and Olbricht, 1996; Manga, 1996). In particular, suspended particles favour the high-flow branches to a greater extent than predicted by the above criterion. If a general law describing this distribution should be found in more systematic studies, it could easily be incorporated into our model. We will see, however, that the detailed partitioning rules have a small effect on macroscopic properties of the two-phase flow.

If the shortest of the times the bubbles would need to reach the end of their tubes is greater than the time until the next bubble enters the network, then the latter time is used to advance the bubbles. Once the bubbles have been moved, the new bubble is added.

Finally, in our simulations we do not account for the possibility of bubble break-up or coalescence. In bubble trains where two bubbles are separated only by a thin lamella of the suspending fluid, coalescence has been observed experimentally to be a very rare event (Ratulowski and Chang, 1989). The break-up of a bubble is most likely when it passes through a constriction. At the center of a constriction, the radius of curvature of the interface between the two fluids is reduced. Surface tension therefore drives the suspending fluid into a growing collar at the centre of the constriction. Eventually this collar can become large enough to form a lamella

of suspending fluid that separates the bubble into two smaller bubbles. While our tubes are straight there are still constrictions in our model porous material at the nodes where tubes of different diameters meet. The main objective of the present study, however, is to investigate the implications of the results regarding a single bubble in a single tube for a larger number of bubbles in a network of tubes, and not to construct a comprehensive theory of porous media that can account for all possible effects. Nevertheless, if an easily parameterized theory describing the break-up of bubbles at nodes is developed, break-up could be incorporated into our simulations.

At this point we should comment on why numerical simulations are necessary for this problem. At large Ca the difference between the bubble speed and mean fluid speed can be large, about 10% for Ca $\approx 10^{-2}$. At small Ca, the difference between the bubble and fluid speed is small; however, the pressure drop across a bubble in a tube will be a substantial fraction of the total pressure drop, and the bubble will thus have a large effect on the flow.

3. Results and Discussion

We begin our simulations with a network free of bubbles. A certain time after the bubbles enter the network a 'steady state' is reached in which the flow rate as well as other physical quantities fluctuate around a mean value, as shown in Figure 2. The flux does not only depend on the number of bubbles in the network: there is no correlation between the fluctuations of the number of bubbles in the network and the flux through the network (correlation coefficient $\simeq 0.1$). All results are presented in dimensionless form, with times normalized by $\bar{r}/\bar{u}$, where $\bar{u}$ is the mean bubble speed.

We characterize our simulations by determining dimensionless *effective permeabilities* as a function of $\overline{\mathrm{Ca}}$ and ϕ. We define the effective permeability k_{eff} as the flux in the presence of bubbles divided by the flux through the same network at the same pressure difference if no bubbles are present. k_{eff} is based on the average flux in steady state. In order to help interpret our results in terms of bubble interactions and dynamics, we made animated movies that show the relative fluxes in each tube as well as the position of each bubble. Copies of the animated video are available from the authors.

3.1. EFFECTS OF NETWORK GEOMETRY AND DIMENSION

As the execution time of our simulations is a rapidly increasing function of the network dimension (see Appendix), we are limited to relatively small networks with up to several hundred tubes. We must therefore determine the extent to which such small networks are representative of the immense networks found in macroscopic porous media. We use random numbers to generate several different networks of a given dimension. All the tubes in all the networks are chosen according to

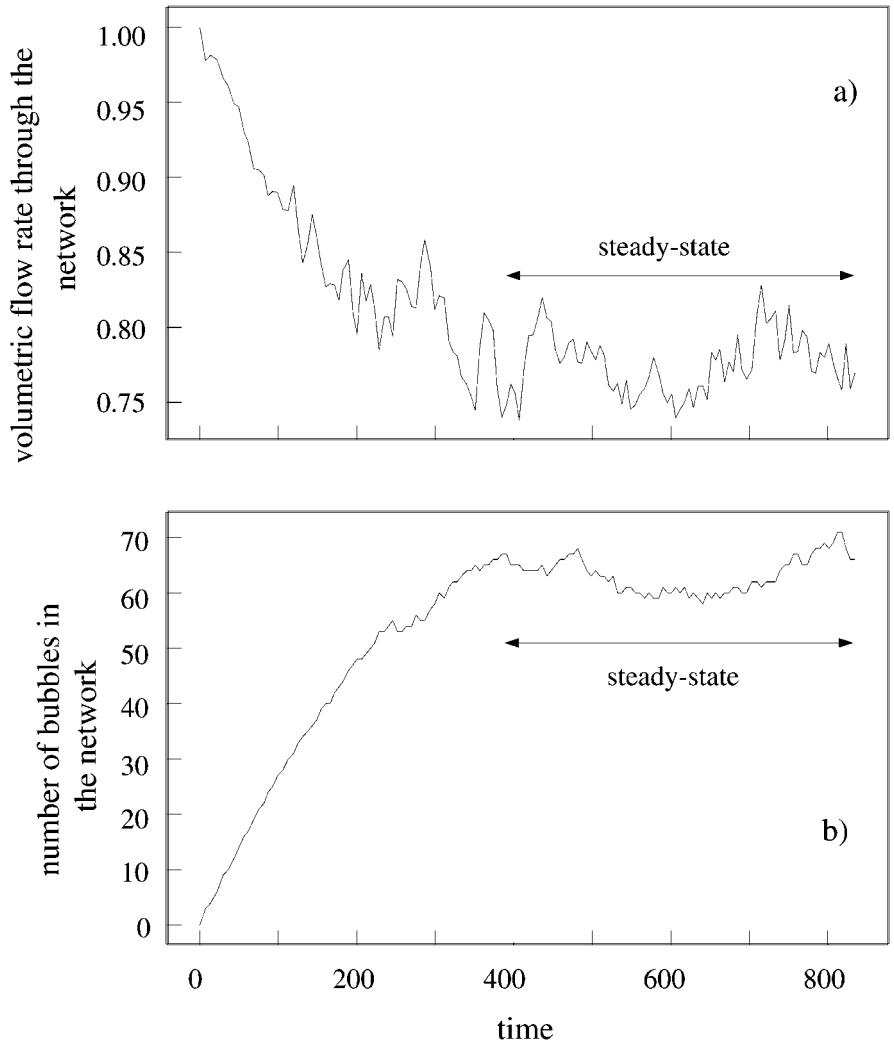

Figure 2. Evolution of (a) flow rate and (b) number of bubbles in the network as a bubbly fluid is introduced into a network. Here $d = 8$, $\phi = 10\%$, and $\overline{\mathrm{Ca}} \simeq 1.4 \times 10^{-4}$. Time is normalized by $\bar{r}/\bar{u}$.

the distribution of probabilities listed in Table I. Figure 3 shows k_{eff} for different network dimensions for the case $\phi = 5\%$ and $\overline{\mathrm{Ca}} \simeq 1.33 \times 10^{-4}$. Each cross represents one particular network and each circle the mean value for all networks of a given dimension. The mean values of k_{eff} for the different dimensions are similar, but the values for the individual networks are widely scattered, especially at low dimension. One of the reasons for this is that the actual distribution of radii in the networks can be quite different from the distribution of probabilities used to create the networks. A network with $d = 2$, for example, consists of only eight tubes, and

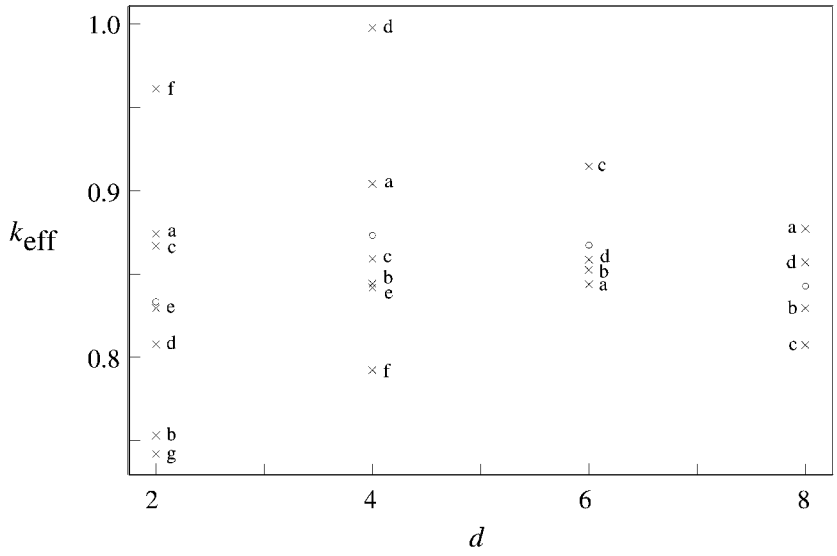

Figure 3. Effective permeability of different networks for $\phi = 5\%$ and $\overline{\text{Ca}} \simeq 1.33 \times 10^{-4}$. The circles show the mean value for all networks at each dimension.

this number is too small to obtain a representative sample of radii. Network number 4*d*, for example, is such that, when no bubbles are present, more than two thirds of the liquid that enters the network leaves through one of the five exit tubes. The capillary number in that tube is more than twice the overall capillary number $\overline{\text{Ca}}$. As the flux through the entire network is heavily influenced by what is happening in that one single tube, the results obtained for network number 4*d* are very different from those obtained for the other networks, even if $\overline{\text{Ca}}$ is the same for all networks.

Figure 4 shows the results of a series of simulations made at $\phi = 5\%$ with network number 4*a* and a corresponding series of simulations made with network number 2*a*. The points for these two networks do not lie on the same curve, but the two curves are close to each other and, more importantly, they have the same form despite the fact that the number of tubes in these two networks differ by a factor of four. With these small networks we may not be able to obtain exact predictions of physical parameters such as k_{eff}, but we still can investigate the general form of the laws describing the evolution of physical parameters under changing conditions.

3.2. EFFECTS OF PARTITIONING CRITERIA

As bubbles arriving at nodes might favour the high-flow branches to a greater extent than predicted by our standard criterion (Ditchfield and Olbricht, 1996; Manga, 1996), we also investigate the effect of the partitioning criterion for bubbles at a node. Figure 4 also shows the results of a series of simulations made using the 'highest-flow criterion'. In these simulations a bubble arriving at a node goes into the tube with the highest flow rate away from the node. The points representing

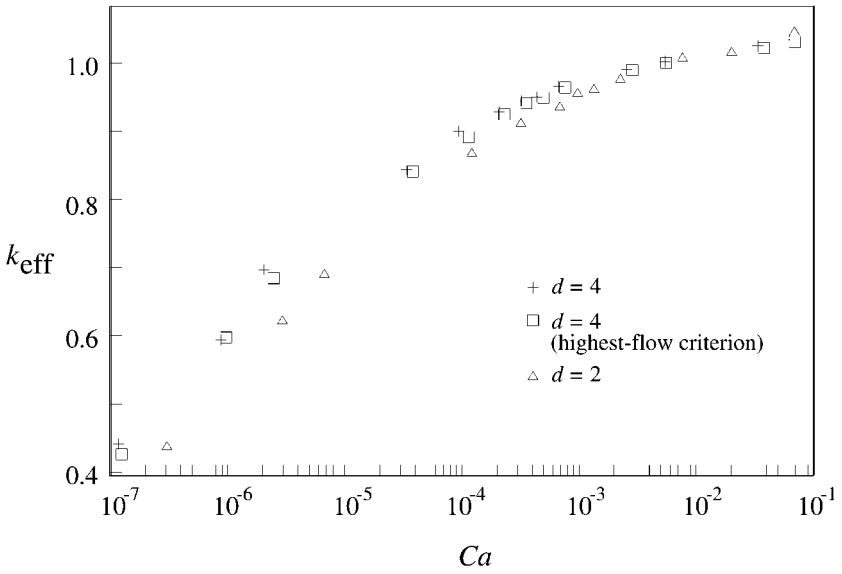

Figure 4. Comparison of results obtained using networks of different dimensions, and different criteria to determine the partitioning of bubbles at nodes; $\phi = 5\%$.

these simulations are nearly coincident with the points representing the simulations made under the same physical conditions and using the same network but with the standard criterion described in Section 2.2. We observe that bubbles have a tendency to end up in the high-flow tubes even if the standard criterion is used. It is thus not astonishing that the use of the highest-flux criterion does not affect the results in a drastic manner. A revision of the criterion might become important if studies of the behaviour of bubbles at trifurcations should show that the low-flux pathways are preferred under certain conditions.

3.3. EFFECTS OF Ca AND ϕ

The effective permeability of network number 4*a* is shown in Figure 5 for different capillary numbers $\overline{\text{Ca}}$ and volume fractions ϕ. At fixed ϕ, k_{eff} is an increasing function of $\overline{\text{Ca}}$. Mathematically this can be understood from Equations (3) and (7). The pressure drop across a bubble is proportional to $\text{Ca}^{2/3}$, whereas the pressure drop across a column of the suspending fluid is proportional to Ca. As can be seen from (10), the pressure drop across the rest of the tube is proportional to Q and therefore proportional to v. As w is always close to zero (especially at small Ca), u and v are nearly the same. At low Ca, ΔP_{b} is thus greater than the pressure drop across a column of the suspending fluid of the same length as the bubble, and it is more difficult to drive the suspension through the network than the suspending fluid. Consequently, k_{eff} is less than one. Physically, a low Ca means that surface tension forces are large compared to viscous forces. Surface tension at the interface

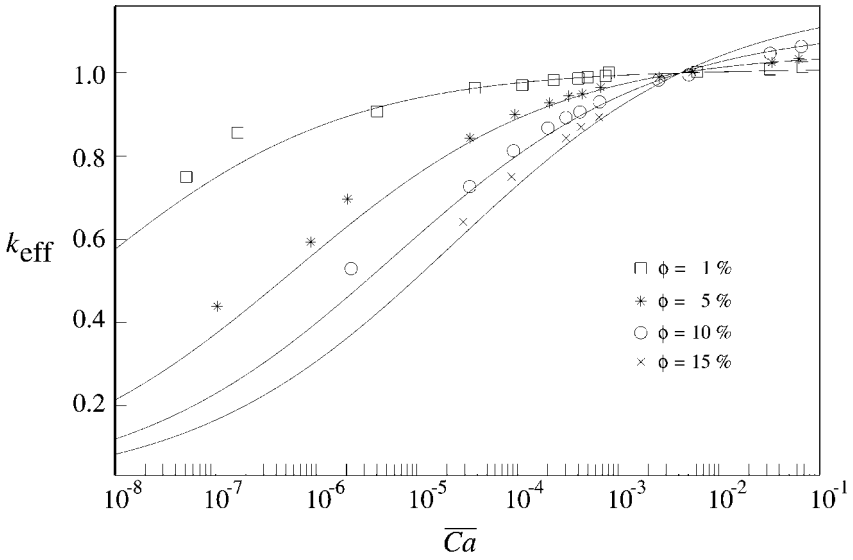

Figure 5. Effective permeability of network number 4*a* as a function of ϕ and $\overline{\mathrm{Ca}}$. The continuous curves represent the predictions for a single unbranched tube, Equation (21).

between the bubble and the suspending fluid offers more resistance to the pressure difference applied between the two reservoirs than the viscous suspending fluid. At high Ca, ΔP_{b} becomes small compared to the pressure drop across a column of the suspending fluid of the same length. Now most of the pressure drops at the parts of the tubes filled with the suspending fluid. This situation is similar to the case in which no bubbles are present, but the tubes that do contain bubbles appear shorter as the parts occupied by bubbles have a negligible contribution to the pressure drop. k_{eff} is almost constant, but greater than one. Physically, a high Ca means that surface tension forces are small compared to viscous forces. If viscous effects dominate, it is easier to drive a viscous fluid containing relatively inviscid bubbles through a network than to drive the pure viscous fluid through it.

The curves for different ϕ all appear to meet near one point at $k_{\mathrm{eff}} \simeq 1$ and $\overline{\mathrm{Ca}} \simeq 6 \times 10^{-3}$. There must be a 'critical' value of Ca (denoted $\mathrm{Ca}_{\mathrm{cr}}$) at which the pressure drop across a bubble is the same as the pressure drop across a column of the suspending fluid of the same length. This $\mathrm{Ca}_{\mathrm{cr}}$ depends on the radius of the tube in question. In a network made of tubes of different diameters there might still be a value of $\overline{\mathrm{Ca}}_{\mathrm{cr}}$ at which the time-averaged pressure drop across a bubble is equal to the corresponding pressure drop across a column of the suspending fluid. This $\overline{\mathrm{Ca}}_{\mathrm{cr}}$ should be independent of the volume fraction as the number of bubbles is unimportant if bubbles and liquid are 'indistinguishable'. At all other values of $\overline{\mathrm{Ca}}$ more bubbles should have a greater effect than few bubbles, and the data points for higher ϕ in Figure 5 are further away from $k_{\mathrm{eff}} = 1$ than those for lower ϕ.

We can estimate the value of $\overline{\mathrm{Ca}}_{\mathrm{cr}}$ at which bubbles and the suspending fluid are indistinguishable. Equations (3) and (7) give the pressure drop across a column of

the suspending fluid and a bubble in a tube of given radius. On the assumption that w is small, u and v are almost identical and the two pressure drops can be expressed as functions of Ca. Equating the two pressure drops leads to the condition

$$\mathrm{Ca}_{\mathrm{cr}} = \left(0.93\frac{\pi}{V_{\mathrm{b}}}\right)^{3} r^{9}. \tag{15}$$

If we let $r = \bar{r}$ (i.e., the average radius of the tubes in our network) we find $\mathrm{Ca}_{\mathrm{cr}} = 8.6 \times 10^{-3}$, which is close to the value of $\overline{\mathrm{Ca}_{\mathrm{cr}}}$ estimated from Figure 5.

Finally, we compare the behaviour of our network with a train of bubbles in a single tube at the same ϕ. Consider N_{b} bubbles of volume V_{b} in a tube of length l and radius r. From geometric considerations we obtain

$$N_{\mathrm{b}} = \frac{\phi\pi r^2 l}{V_{\mathrm{b}}}, \tag{16}$$

and the length of the tube minus the combined lengths of the bubbles in it is

$$l^* = l(1-\phi). \tag{17}$$

In order to calculate the effective permeability, we begin with the condition that the pressure drop ΔP across the tube in the absence of bubbles is the same as the sum of the total pressure drop across the bubbles, ΣP_{b}, and the total pressure drop across the regions filled with the suspending fluid, ΣP_{w}:

$$\Delta P = \Sigma \Delta P_{\mathrm{b}} + \Sigma \Delta P_{\mathrm{w}}. \tag{18}$$

Assuming that the speed of the bubbles u is close to the average speed of the liquid v, we have

$$\mathrm{Ca} = \frac{\mu}{\sigma}\frac{Q}{\rho\pi r^2}. \tag{19}$$

Substituting (3), (7) and (19) into (18) yields

$$\frac{8\mu l}{\pi\rho r^4}Q_0 = \frac{8\mu l^*}{\pi\rho r^4}Q + N_{\mathrm{b}}\,3.58\frac{\sigma}{r}\left(3\frac{\mu}{\sigma}\frac{Q}{\rho\pi r^2}\right)^{2/3}, \tag{20}$$

where Q_0 is the flow rate in the absence of bubbles. Dividing (20) by Q and using $k_{\mathrm{eff}} = Q/Q_0$ we obtain

$$k_{\mathrm{eff}} = 8\left[8(1-\phi) + \frac{\phi\pi r^3}{V_{\mathrm{b}}}\cdot 3.58\cdot 3^{2/3}\mathrm{Ca}^{-1/3}\right]^{-1}. \tag{21}$$

Notice that (21) does not depend on the length of the tube. k_{eff} given by (21) is shown with the continuous curves in Figure 5 for bubbles with the same volume (relative to $\bar{r}$) as those used in the numerical simulations.

The predictions for one tube and the predictions of our network simulations are remarkably close, especially at high $\overline{\mathrm{Ca}}$ and low ϕ. This is consistent with the

observation that the bubbles tend to end up in high-flow pathways. These high-flow pathways winding through the network can be compared to a bundle of straight and independent capillary tubes, despite the fact that they can contain some tubes that are perpendicular to the main direction of the flow and that tubes are interconnected. While there is a small flux of the suspending fluid from one high-flow pathway to another, most of the bubbles remain on a given high-flow pathway. This phenomenon is especially marked at low ϕ, that is, when few bubbles are present. At higher ϕ, the interactions between individual bubbles become more important. At low $\overline{\mathrm{Ca}}$, the presence of one or more bubbles on a high-flow pathway can significantly reduce the flow through that pathway. Other bubbles are thus more likely to leave that high-flow pathway, and the presence of nodes enables bubbles to avoid congested pathways. At fixed $\overline{\mathrm{Ca}}$, we thus expect the differences between our simulations and the predictions for one single capillary tube, Equation (21), to increase as ϕ increases. At fixed ϕ we expect the differences between simulations and predictions to decrease as $\overline{\mathrm{Ca}}$ increases. These two trends can be observed in Figure 5.

3.4. RESIDENCE TIME OF BUBBLES IN THE NETWORK

The interaction phenomena described previously also affect the time it takes for individual bubbles to traverse the network. We define the transit time or residence time of a given bubble as the time the bubble spends in the network. Figure 6 shows histograms of the residence times of bubbles in two simulations made using the same network (number 4*a*) and $\overline{\mathrm{Ca}} = 2.0 \times 10^{-4}$, but with different volume fractions ($\phi = 1\%$ and 10%). The form of the two histograms is similar; however, the distribution of residence times for the higher ϕ simulation is wider. In particular, a greater fraction of bubbles have shorter transit times, and the tail of the distribution is extended. The shorter transit times reflect the increased flux through the highest flow pathway due to bubbles 'blocking' the low-flux (and thus low Ca) tubes. The long transit times are due to bubbles that are forced into these low-flow tubes. The (dimensionless) mean transit times, nevertheless, are similar: 123 and 118 for the $\phi = 1\%$ and 10% simulations, respectively. In animated videos we can also observe 'trapped' bubbles, that is, bubbles that enter, but do not leave, low-flow tubes.

4. Concluding Remarks

The present study is motivated by a desire to extend results based on bubbles in a single tube to a network of tubes that is more representative of real porous materials with connected porosity. Here we have considered dilute suspensions of long bubbles that are not permitted to coalesce and break-up. In principle, given appropriate parameterizations for coalescence, break-up, and partitioning at nodes, more realistic and complicated phenomena involving suspensions can be simulated. Unfortunately, the nonlinear relationship between the flux and capillary number limits

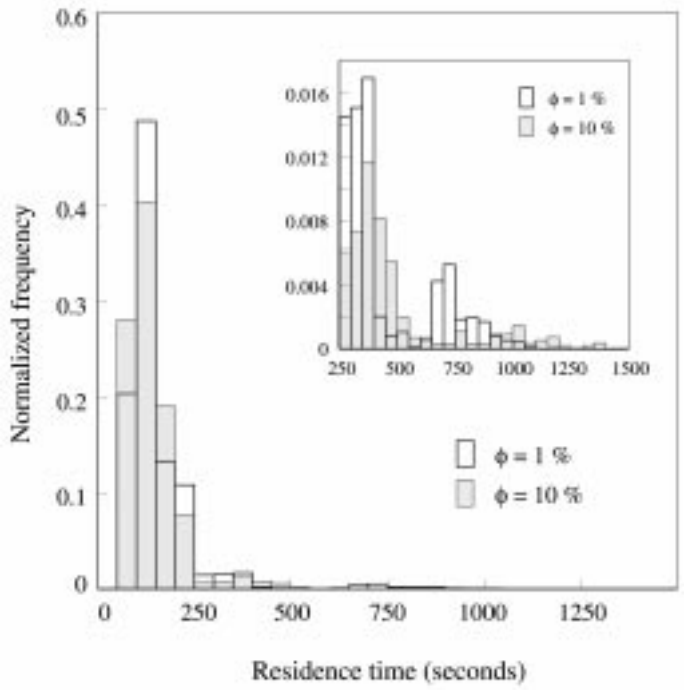

Figure 6. Histogram of the residence times of bubbles in simulations made at $\phi = 1\%$ and 10% (bold lines and shaded bars, respectively). In both cases $\overline{\mathrm{Ca}} \simeq 2.0 \times 10^{-4}$. Histograms are normalized by the number of bubbles counted (3.4×10^4 and 5.6×10^3 for the simulations with $\phi = 1\%$ and 10%, respectively). Inset shows the tails of the residence time distributions. Time is normalized by $\bar{r}/\bar{u}$.

the size of the networks that can be simulated. Our network simulations, however, allow us to obtain information that is difficult to obtain experimentally. For example, the distribution of transit times for steady flows would be difficult to determine in experiments (though breakthrough curves can be generated for transient problems).

Models for single phase flow in porous materials that represent the material as a bundle of independent tubes lead to simple analytical expressions that describe many aspects of real flows. Our results show that this simple geometrical model can be extended to include aspects of the flow of bubbly liquids through porous media at low bubble volume fractions. This extension leads to approximate analytical equations than could be useful for certain applications.

Appendix

In electronics, all currents and voltage drops in a network of resistors can be calculated using Kirchhoff's rules. These rules, which are essentially a restatement of the conservation of electric charge and of energy, provide a complete set of linear

equations that can be solved by performing a matrix inversion. Using the analogy between a tube containing bubbles and a resistor, Equation (14), we can apply Kirchhoff's rules to our network of tubes. In terms of this analogy, the conservation of electric charge corresponds to the conservation of fluid mass. But the equations we obtain are no longer linear as the conductivities are now complicated functions of the flux and the pressure drop. The standard techniques used to solve systems of linear equations, such as matrix inversion are no longer sufficient, and require suitable iterative algorithms (e.g., Lenormand *et al.*, 1988; Mogensen and Stenby, 1998). In this appendix, we outline the approaches we use to determine the flux and pressure distribution in the network for a given configuration of bubbles.

We choose a set of conductivities to start the iteration process, e.g., the conductivities the tubes would have if no bubbles are present. We then solve the corresponding system of linear equations to obtain the fluxes Q and the total pressure drop across the bubbles ($\sum_{\text{bubbles}} \Delta P_{\text{b}}(Q)$) in each tube corresponding to these fluxes. For each tube we thus obtain a new conductivity that can be used as input for the next iteration. Hopefully, the differences between the currents calculated in two successive iterations become smaller with each step, and the algorithm converges.

In most cases, the changes of the fluxes from one timestep to another are very local. That is, when a bubble enters a new tube the fluxes in its immediate vicinity are affected, but in general, the impact on the fluxes in tubes far away from the bubble is small. Thus, it is much more efficient to use the solution of the previous timestep as input for the first iteration. The conductivity of tubes that no longer contain bubbles in the new timestep is set to the 'no bubble'-value.

This simple procedure would be very effective if the pressure drop across the bubbles is a small correction to the pressure drop across the rest of the tube. This is not necessarily the case. On the contrary, we encounter many configurations in which the pressure drop across the bubbles in a given tube is more than one hundred times higher than the pressure drop across the rest of the tube. The pressure drop across a bubble is proportional to $\text{Ca}^{2/3}$ for the corresponding tube and, as can be seen from the definition of Ca, proportional to $u^{2/3}$. The pressure drop across the rest of the tube is proportional to Q and therefore proportional to v. As Ca decreases, the pressure drop across a bubble therefore increases faster than the pressure drop across the rest of the tube. Even when $\overline{\text{Ca}}$ is large, there can still be some tubes in which the flow is very slow, i.e., locally the capillary number can still be very small.

In most cases the simple iteration procedure described above does not converge. Two specific improvements allow us to find a useful numerical solution for all configurations of bubbles except some very rare problematic situations at high ϕ.

1. When a bubble enters a new tube, the flux in the tube the bubble leaves is likely to increase, and the flux in the tube the bubble enters is likely to decrease. If we use the solution of the previous timestep as the starting point for our iterations, the flux in the tube the bubble enters is overestimated. Consequently, the pressure drop across the bubbles in that tube is also overestimated. In some

situations it is so severely overestimated that the new conductivity calculated by the iterative process would be negative. Experience shows that finding a solution is particularly complicated when this problem occurs in several tubes at the same time. The solution to this problem, that works most of the time, comes from electronics. Fragile electronic components frequently have to be protected from high currents that would destroy them. This can be achieved using *protective resistors* that increase the total resistance of a fragile circuit and thereby reduce the current that flows through it. We apply the same concept to our problem: we initially do not only lower the conductivity of the tube that causes the trouble, but also the conductivity of the tubes that are directly connected to it.

2. There is a nonnegligible number of configurations in which the 'protective resistors'-method does not lead to convergence. In these cases we use a different approach that turns out to be very powerful, but also requires an enormous number of iterations. It could be summarized as 'cutting the trouble tubes out and making them reappear slowly'. The conductivities of the tubes in which the problem appeared are assigned values very close to zero, and the solution for this new configuration is calculated using the above techniques. This solution is then used as input for a new iteration process in which the conductivity of the trouble tubes is subsequently increased in very small steps. At the end of this process the conductivities of the trouble tubes are allowed to evolve freely again.

For many configurations a solution can be found in as few as 10 iterations. In a few cases up to several tens of thousands of iterations can be required. Not only can convergence be slow, it is often necessary to try several variants of the iterative algorithm to achieve convergence. Each iteration requires one matrix inversion. The time required for a matrix inversion is approximately $O(N^3)$, where N is the dimension of the square matrix to be inverted. We need as many equations as there are tubes in our network, and the number of tubes is $O(d^2)$, so that the total computational effort per inversion is $O(d^6)$. Profiling indicates that our simulation times are largely dominated by matrix inversion. Typical running times are 2 h at $d = 4$ and several days at $d = 8$ on a Sun Ultra Sparc processor, with computation time increasing as ϕ increases and Ca decreases.

Acknowledgements

Work supported by NSF grant EAR-9701768. The authors thank the reviewers for thoughtful comments.

References

Avraam, D. G. and Payatakes, A. C.: 1995, Flow regimes and relative permeabilities during steady-state two-phase flow in porous media, *J. Fluid Mech.* **293**, 207–236.

Babchin, A. J. and Yuan, J.-Y.: 1997, On the capillary coupling between two phases in a droplet train model, *Transport in Porous Media* **26**, 225–228.

Babchin, A. J., Frenkel, A. L., Levish, B. G. and Sivashinky, G. I.: 1983, Nonlinear saturation of Rayleigh–Taylor instability in thin films, *Phys. Fluids* **26**, 3159–3161.

Böhler, U., Brauns, J., Hötzl, H. and Nahold, M.: 1990, Air injection and soil air extraction as a combined method for cleaning contaminated sites – observations from test sites in sediments and solid rocks, In: F. Arendt, M. Hinsenveld and W. J. van den Brink (eds), *Contaminated Soil '90*, Kluwer Academic Publishers, Norwell, Massachusetts, pp. 1039–1044.

Borhan, A. and Mao, C. F.: 1992, Effect of surfactants on the motion of drops through circular tubes, *Phys. Fluids A* **4**, 2628–2640.

Borhan, A. and Pallinti, J.: 1999, Break-up of drops and bubbles translating through cylindrical capillaries, *Phys. Fluids* **11**, 2846–2855.

Bretherton, F. P.: 1961, The motion of long bubbles in tubes, *J. Fluid Mech.* **10**, 166–188.

Celia, M. A., Reeves, P. C. and Ferrand, L. A.: 1995, Recent advances in pore scale models for multiphase flow in porous media, *Rev. Geophys.* **33**, 1049–1057.

Constantinides, G. N. and Payatakes, A. C.: 1996, Network simulation of steady-state two-phase flow in consolidated porous media, *AIChE J.* **42**, 369–382.

Dias, M. M. and Payatakes, A. C.: 1986, Network models for two-phase flow in porous media. 1. Immiscible microdisplacement of non-wetting fluids, *J. Fluid Mech.* **164**, 305–336.

Ditchfield, R. and Olbricht, W. L.: 1996, Effects of particle concentration on the partitioning of suspensions at small divergent bifurcations, *J. Biomech. Engng* **18**, 287–294.

Foulser, R. W. S., Goodyear, S. G. and Sims, R. J.: 1991, New concepts in relative permeabilities at high capillary numbers for surfactant flooding, *Transport in Porous Media* **6**, 223–240.

Frenkel, A. L., Babchin, A. J., Levich, B. G., Shlang, T. and Sivashinky, G. I.: 1987, Annular flows can keep unstable films from break-up: Nonlinear saturation of capillary instability, *J. Colloid Interface Sci.* **115**, 225–233.

Fry, V. A., Selker, J. S. and Gorelick, S. M.: 1997, Experimental investigations for trapping oxygen gas in saturated porous media for *in situ* bioremediation, *Water Resour. Res.* **33**, 2687–2696.

Gudemann, H. and Hiller, D.: 1988, *In situ* remediation of VOC contaminated soil and groundwater by vapor extraction and groundwater aeration, In: *Proceedings of the Third Annual Haztech International Conference*, Haztech Int., Cleveland, Ohio, pp. 2A90–2A111.

He, Z., Dagan, Z. and Maldarelli, C.: 1991, The influence of surfactant adsorption on the motion of a fluid sphere in a tube. Part 1. Uniform retardation controlled by sorption kinetics, *J. Fluid Mech.* **222**, 1–32.

Koplik, J. and Lasseter, T. J.: 1982, Two-phase flow in random network models of porous media, *Soc. Petr. Engng J.* **2**, 89–100.

Lenormand, R., Touboul, E. and Zarcone, C.: 1988, Numerical models and experiments on immiscible displacements in porous media, *J. Fluid Mech.* **189**, 165–187.

Manga, M.: 1996, Dynamics of drops in branched tubes, *J. Fluid Mech.* **315**, 105–117.

Martinez, M. J. and Udell, K. S.: 1990, Axisymmetric creeping motion of drops through circular tubes, *J. Fluid Mech.* **210**, 565–591.

Mogensen, K. and Stenby, E. H.: 1998, A dynamic two-phase pore-scale model of imbibition, *Transport in Porous Media* **32**, 299–327.

Olbricht, W. L.: 1996, Pore-scale prototypes of multiphase flow in porous media, *Ann. Rev. Fluid Mech.* **28**, 187–213.

Olbricht, W. L. and Kung, D. M.: 1992, The deformation and breakup of liquid drops in low Reynolds number flow through a capillary, *Phys. Fluids A* **4**, 1347–1354.

Rajaram, H., Ferrand, L. A. and Celia, M. A.: 1997, Prediction of relative permeabilities for unconsolidated soils using pore-scale network models, *Water Resour. Res.* **33**, 43–52.

Ratulowski, J. and Chang, H.-C.: 1989, Transport of gas bubbles in capillaries, *Phys. Fluids A* **1**, 1642–1655.

Ratulowski, J. and Chang, H.-C.: 1990, Marangoni effects of trace impurities on the motion of long gas bubbles in capillaries, *J. Fluid Mech.* **210**, 303–328.

Teletzke, G. F., Davis, H. T. and Scriven, L. E.: 1988, Wetting hydrodynamics, *Revue Phys. Appl.* **23**, 989–1007.

Tsai, T. M. and Miksis, M. J.: 1994, Dynamics of a drop in a constricted capillary tube, *J. Fluid Mech.* **274**, 197–217.

Wong, H., Radke, C. J. and Morris, S.: 1995a, The motion of long bubbles in polygonal capillaries. 1. Thin films, *J. Fluid Mech.* **292**, 71–94.

Wong, H., Radke, C. J. and Morris, S.: 1995b, The motion of long bubbles in polygonal capillaries. 2. Drag, fluid pressure and fluid flow, *J. Fluid Mech.* **292**, 95–110.